Microstructure and its effect on field electron emission of grain-size-controlled nanocrystalline diamond films

Kehui Wu, E. G. Wang,[a] and Z. X. Cao
State Key Laboratory for Surface Physics, Institute of Physics, Chinese Academy of Sciences, Beijing 100080, People's Republic of China

Z. L. Wang
School of Materials Science and Engineering, Georgia Institute of Technology, Atlanta, Georgia 30332-245

X. Jiang
Fraunhofer-Institut fur Schicht- und Oberflachentechnik, Bienroder Weg 54E, D-38108 Braunschweig, Germany

(Received 22 November 1999; accepted for publication 31 May 2000)

Nanocrystalline diamond films were grown by microwave plasma assisted chemical vapor deposition using N_2 and CH_4 as precursors. The microstructure of the films such as the diamond grain size, graphite content, and N incorporation, was controlled by introducing a small amount of hydrogen gas (0–10 sccm) in the growth. Effects of the growth parameters on the film microstructure were investigated using transmission electron microscopy, x-ray diffraction, Raman spectroscopy, and secondary ion mass spectroscopy. A surface stabilizing model is suggested to explain the formation mechanism of the uniformly grain size-controlled nanocrystalline diamond. A systematic investigation on the film microstructure and their field electron emission (FEE) property is presented for various films of different diamond grain sizes and graphite contents. It was found that the FEE property highly depended on the diamond/graphite mixed phase structure. Novel field emission properties (1 V/mum emission threshold and 10 mA/cm^2 emission current) are obtained by optimizing the growth parameters. A transport-tunneling mechanism is applied to explain the experimental observations. Our results showed that nanocrystalline diamond film can be a very promising cold cathode material for field emission applications. © *2000 American Institute of Physics.* [S0021-8979(00)07117-6]

I. INTRODUCTION

Diamond and related materials have been extensively studied for their novel mechanical, chemical, and electrical properties. Particularly, because of its low or negative electron affinity (NEA),[1] diamond is an optimum candidate for field electron emission (FEE), which has potential applications in the areas such as flat panel display and microelectronic devices. Cold cathode field emission has been demonstrated in chemical vapor deposited (CVD) polycrystalline diamond films,[2–7] from which a prototype flat panel display has even been made.[8] However, the mechanism of electron emission from CVD diamond films remains to be investigated, although several models have been suggested, such as the surface morphology,[3] back-metal contact,[4] surface diode,[5] and defect-induced energy band.[7,9] The variety of models is likely to be the result of a wide range of CVD diamond films with distinct surface morphology, conductance, impurity, and back contact characteristics. A paradox is that diamond films with poor quality gives good FEE properties, making the problem more complex.

In the undoped CVD diamond films, the conductance of the bulk is limited by the space-charge-limited-current.[10] As a result, grain boundaries, which are highly disordered and may contain codeposited graphitic impurities, have been suggested as the main conducting pathway. Because reduction in diamond grain size may increase the conducting pathways, it is possible to improve diamond FEE by depositing size controlled diamond films. Because of this and other unique features, such as low friction[11] and high transparency,[12] nanocrystalline diamond films are rather attractive. Zhou *et al.*[13] have grown nanocrystalline diamond films by plasma enhanced CVD, with an emission threshold of about 3 V/μm. Zhu *et al.*[7] observed a threshold as low as 1 V/μm in diamond films prepared from industrial diamond nanopowders. Unfortunately, there hasn't been a systematic study on the influence of microstructure on their FEE characteristics of nanocrystalline diamond films. Previous studies on nanocrystalline diamond used $C_{60}/Ar/H_2$, or O_2/Ar addition into the H_2/CH_4 precursors during the CVD process.[14] Controlling the structure of the as-deposited diamond films in these cases proved to be difficult, and the mechanism of field emission from nanocrystalline diamond film is far from being understood.

In this article, we present a systematic study on the synthesis and FEE characterization of nanocrystalline diamond films grown by microwave plasma enhanced CVD (MPCVD) using N_2/CH_4 as precursors. The film microstructure, including diamond grain size and the content of graphite impurity, can be well controlled by deposition param-

[a]Author to whom correspondence should be addressed; electronic mail: egwang@aphy.iphy.ac.cn

eters. A surface stabilizing model is proposed to explain the formation mechanism of nanocrystalline diamond films. Diamond films with different grain sizes (8–50 nm) and graphite content (0%–40%) have been produced for a systematic FEE study. The FEE properties of the nanocrystalline diamond films are found to be highly dependent on their microstructure. By applying a conducting–tunneling model to the nanodiamond/graphite mix-phase films, we have explained the experimental observations from the FEE measurements.

II. EXPERIMENTS

Film deposition was carried out using an ASTeX 2115 microwave plasma CVD system, of which the maximum microwave output power is 1500 W.[15] High purity hydrogen (99.999%), nitrogen (99.999%), and methane (99.9%) gases were employed as precursors. Polycrystalline molybdenum and (100) oriented Si wafers were used as substrates, which were first polished by 1.0 μm diamond paste and then ultrasonically cleaned in acetone, ethanol, and de-ionized water in turn. The main growth parameters are as follows: total ambient pressure 30 Torr, input microwave (2.45 GHz) power 800 W, and the substrate temperature about 600 °C. Two sets of films were grown in our experiments. The first series was prepared with only N_2/CH_4 as precursors where the CH_4 was varied from 2.1 to 8.4 sccm. The second series was grown by introducing 0–10 sccm H_2 gas into the precursors, while the CH_4 was fixed at 3.5 sccm. In all of the experiments the nitrogen flow rate was controlled at 150 sccm.

Transmission electron microscopy (TEM) images were recorded at 200 kV using a Hitachi HF-2000. X-ray diffraction (XRD) was measured by a Rigaku D/max-2400 system using the 0.154 nm Cu $K\alpha$ line. A scan rate of 1°/min from 40° to 80° is used for detailed analysis of the diamond (111) diffraction peak. Raman spectra were recorded using a Renishaw 2000 spectrometer, with the incident laser radiation of 514 nm and power of 12 mW. Secondary ion mass spectra (SIMS) were measured on a CAMECA ims $4f$, using 10 keV positive Cs ion.

The FEE experiments were carried out in a high vacuum system with a base pressure better than 5×10^{-7} Pa. The films which acted as the cathode were mounted on a metal base. A molybdenum probe with its tip area of 1 mm^2 controlled by a stepper was used as the anode. During our experiments the anode–cathode distance was kept constant at 100 μm. The current–voltage (I–V) characteristics of the films were measured by varying the applied voltage, and the emission current was recorded by a Keithley 617 nanoamper meter. For each film several randomly distributed regions were selected for measurements.

III. RESULTS AND DISCUSSIONS

A. Films grown by only CH_4/N_2 as precursors

All of the as-deposited films in our experiments exhibit very smooth surfaces. The first series of films was grown using 2.1–8.4 sccm CH_4, and the N_2 flow was kept at 150 sccm and no H_2 was introduced. The as-grown films show deep black color under visible light. Figures 1(a) and 1(b) show the TEM images of the films grown with 3.5 and 2.1 sccm CH_4, respectively, where a select-area diffraction (SAD) pattern is inserted. The TEM images reveal the nanocrystalline nature of our films. Film (a) has a smaller grain size of ~8 nm. From the average size of the nanocrystals and the average distance between the nanocrystals, the content of amorphous carbon is estimated to be ~40% from the image. The SAD shows a typical ring pattern of nanocrystalline diamond. Film (b) has a larger grain size of about 20–30 nm, and the content of amorphous carbon is obviously reduced.

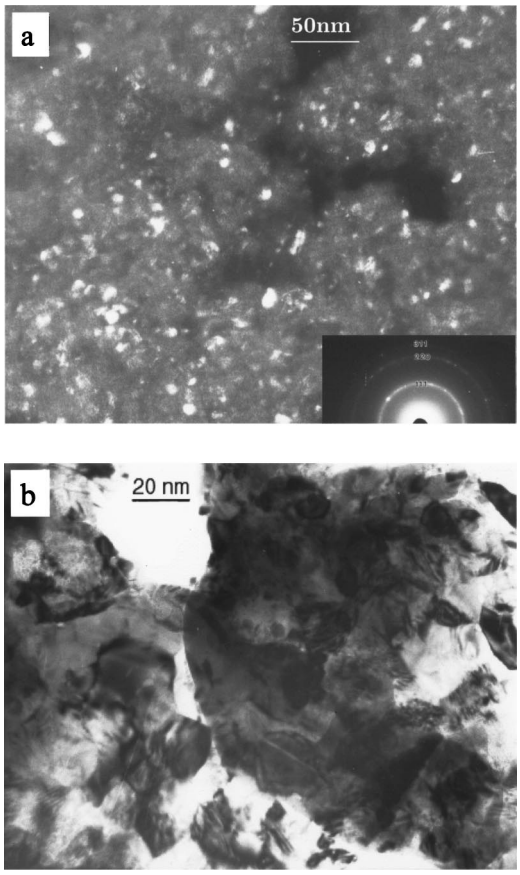

FIG. 1. TEM images of the nanocrystalline diamond films grown with only N_2/CH_4, where (a) and (b) are grown with 3.5 and 2.1 sccm CH_4, respectively. Inserted in the images are the SAD patterns.

XRD spectra in Fig. 2 show strong diamond (111) and (220) feature peaks, where the full width at half maximum (FWHM) of these peaks is significantly broaden due to the small size of the diamond grains. The broadening of diamond peaks provides a way to determine the average diamond grain size in the films. According to the Scherrer equation

$$D=\frac{\lambda}{B\cos\theta},$$

where D is the average grain size, λ the x-ray wavelength, B the integral width of the peak, and θ the Bragg angle.[16] The strongest (111) line is taken for detailed analysis using a Gaussian fitting. For the series of films grown with different CH_4 concentration, the calculated diamond grain size is shown in Fig. 3. It is found that between 8.4 and 3 sccm of CH_4 flow rate, the average diamond grain size does not show

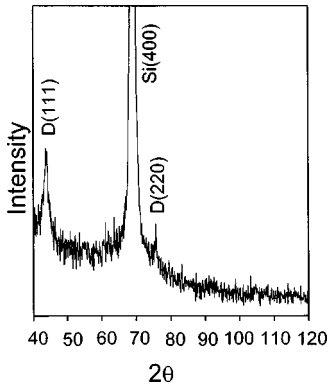

FIG. 2. XRD spectra of the as-grown nanocrystalline diamond films on Si(100). The diamond (111) and (220) diffraction peaks are shown with broaden FWHM.

any significant variation. However, as the CH_4 flow rate is reduced below 3 sccm, the diamond grain size increases, consistent with the TEM results, although, the actual values obtained by these two methods are not exactly the same, probably because of the residual stress and defects in the films.

Raman spectra of this series of films are shown in Fig. 4. They consist of two main peaks around 1560 and 1350 cm^{-1}, corresponding to the *G* and *D* bands of graphite, respectively. This confirms the existence of graphite phase in our films as observed by TEM. Special attention should be paid to the additional peak at ~1150 cm^{-1}, which is caused by size effect of the nanoscale diamond grains,[17,18] and provides more evidence for the nanocrystalline nature of our films. We find that this peak becomes weaker with decreasing CH_4 concentration, indicating an increased average diamond grain size. The 1332 cm^{-1} diamond peak is relatively weak in these films, even unrecognizable in some films grown with a high CH_4 concentration. This is because graphite has a much higher resonance cross section than diamond and the graphite content in these films is high. In the films grown with

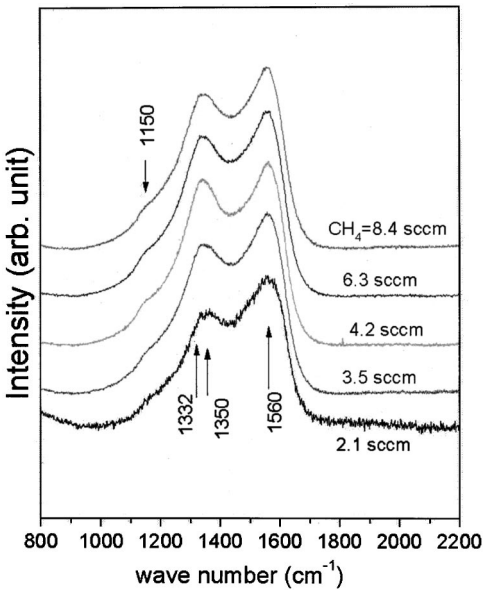

FIG. 4. Raman spectra of nanocrystalline diamond films grown with different CH_4 concentration.

lower CH_4 concentration, such as 2.1 sccm, the 1332 peak is enhanced, showing that the film has a lower graphite content. These results are consistent with the TEM and XRD results.

To study the influence of CH_4 concentration on the film growth rate, the film thickness is measured by a profile meter, and the film growth rate is calculated by dividing the film thickness by the growth time. Figure 5 shows the growth rate as a function of CH_4 concentration. The growth rate decreases nearly linearly with CH_4 concentration. When the CH_4 flow rate is reduced to about 1.5 sccm, there is completely no film growth, only an etching effect of the substrate is found. This is in contrast to the polycrystalline diamond films deposited by the H_2/CH_4 as precursors, whose diamond films can be grown even with very low CH_4 concentration, such as 0.5%.

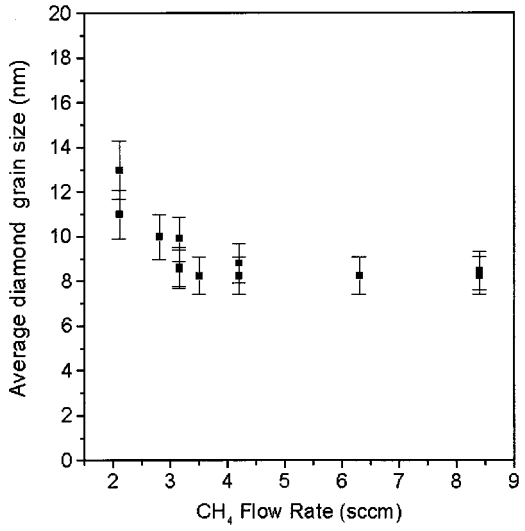

FIG. 3. Influence of CH_4 concentration on the diamond grain size in the films grown with only N_2/CH_4 as precursors.

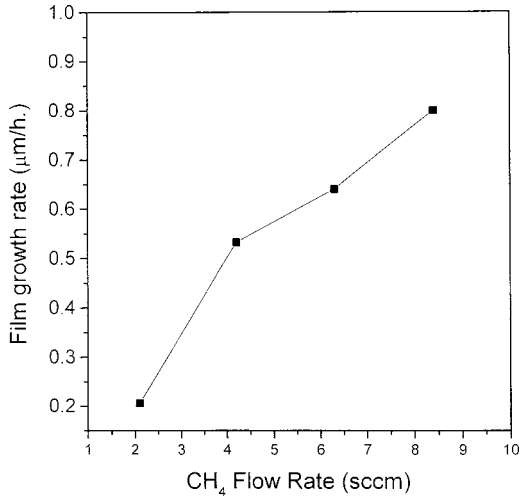

FIG. 5. Influence of the CH_4 concentration on film growth rate.

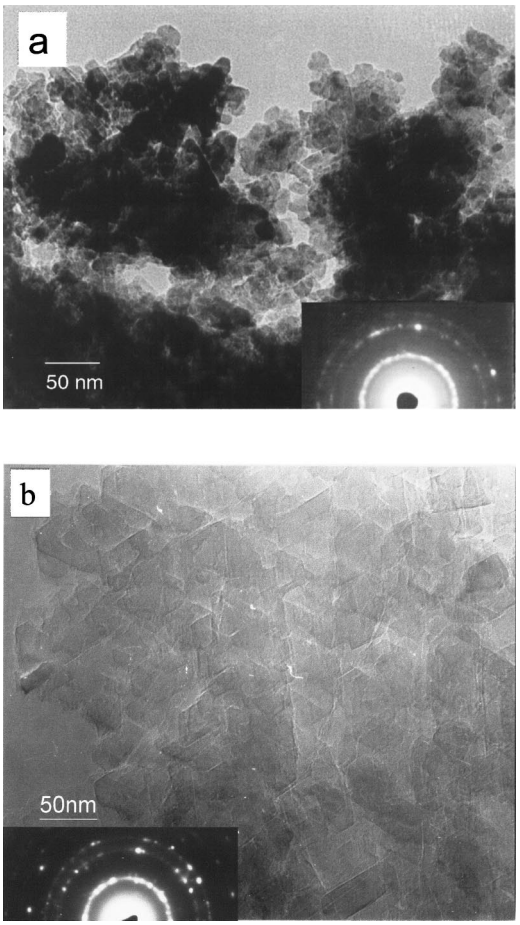

FIG. 6. TEM images of the films grown with H_2 flow rate at: (a) 5.0 and (b) 10.0 sccm, respectively, in which the CH_4 was fixed at 3.5 sccm.

B. Effect of H_2 on film microstructure

In order to further control the microstructure of the nanocrystalline diamond films, we then introduced a small amount of hydrogen gas (0–10 sccm) to the precursors as a new deposition parameter. Figures 6(a) and 6(b) show the TEM images of the films grown with 5.0 and 10.0 sccm H_2, respectively, where the CH_4 is fixed at 3.5 sccm. In comparison with Fig. 1(a), where the same conditions are used but without H_2, a number of differences are observed. First, with increasing of H_2 flow rate, the diamond grain size increases from ~8 to ~20 nm (5 sccm H_2), and then to ~50 nm (10 sccm H_2). Second, graphite is greatly reduced, and nearly pure nanocrystalline diamond films are shown in the images. In fact, it can be observed that with the increase of H_2 flow rate, the film color changes significantly from deep black to gray and then to transparent under visible light. This means that pure nanocrystalline diamond films with controllable grain size were achieved by adjusting the H_2 concentration.

XRD and Raman spectra also confirm these results. Figure 7 shows the detailed XRD information of the diamond (111) peak of the films grown with different H_2 flow rate. There is a very clear evolution of the peak width: the FWHM decreases very quickly with the increase of H_2 flow rate. Shown in Fig. 8 is the average diamond grain size calculated

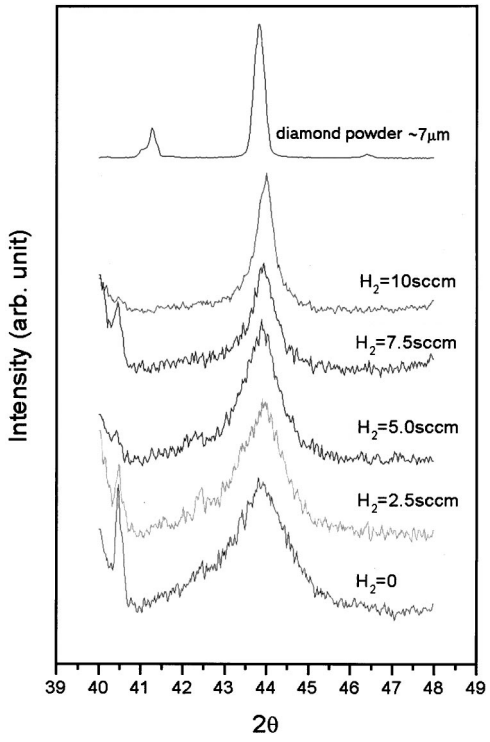

FIG. 7. Influence of H_2 flow rate on the XRD spectra of the diamond (111) main peak.

by the Sherrer equation. It can be seen that, when the H_2 flow increases from 0 to 10 sccm, the average diamond grain size increases from 8 to about 50 nm. The values are consistent with those estimated from TEM images.

Figure 9 shows Raman spectra of this series of films. The relative strength of the 1332 cm^{-1} diamond peak to the graphite bands (*G* band at 1560 cm^{-1} and *D* band at 1350 cm^{-1}) increases significantly with increasing H_2 flow rate. This means that the graphite content is greatly reduced. Furthermore, the peak at 1150 cm^{-1}, which is an indication of the nanosize diamond crystallites, disappears in the films grown with a higher H_2 flow rate, such as 7.5 and 10.0 sccm.

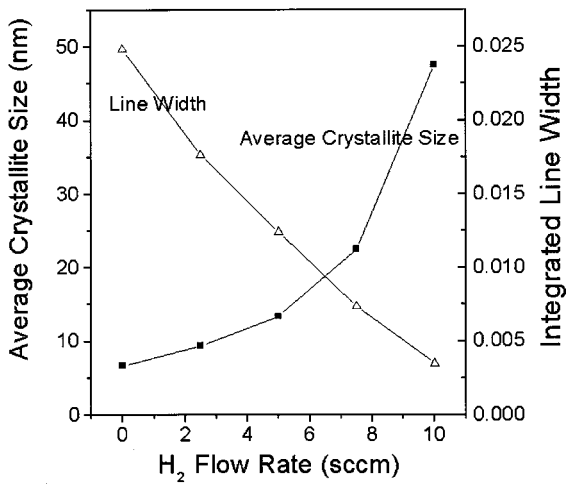

FIG. 8. Influence of H_2 flow rate on diamond grain sizes in the nanocrystalline diamond films, which is calculated from the XRD (111) peak using the Sherrer equation.

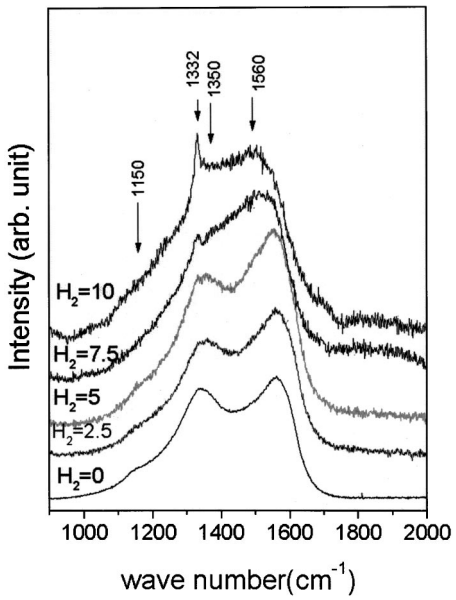

FIG. 9. Raman spectra of the nanocrystalline diamond films grown with H_2 flow rate of 0–10 sccm.

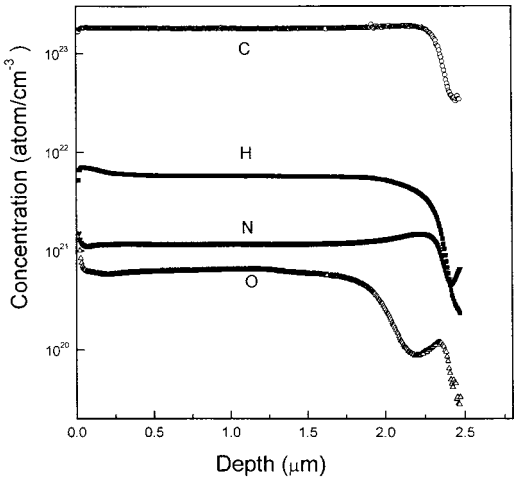

FIG. 10. Typical SIMS results of nanocrystalline diamond films.

This means that, when the diamond grain size increases above some threshold value, its nanoscale features gradually disappear. Estimating from the Raman results, this value should be in the range of 15–25 nm.

Based on the above analysis, we may conclude the following: (1) the microstructure of nanocrystalline diamond films can be controlled by either the CH_4 concentration or the H_2 concentration; and (2) by introducing H_2 gas as an independent adjustable parameter, a stronger control of the film microstructure can be achieved. Our results show that the diamond grain size can be adjusted in the range of about 8–50 nm, and the graphite impurity can be almost completely eliminated from the films.

The film growth rate of this series of films decreases with the increase of H_2 flow rate. When the H_2 flow rate increases to 15 sccm, no film growth but only etching effect of the substrate is observed.

C. Incorporation of nitrogen

SIMS were measured in a CAMECA ims $4f$, with 10 keV positive Cs ions. Both series of films are highly doped with nitrogen, irrespective of the CH_4 concentration or the H_2 flow rate. The dopant concentrations are around $10^{21}\,cm^{-3}$ for all of the films measured. Figure 10 shows a typical SIMS spectrum.

D. Film growth mechanism

Most of the previous studies on the synthesis of diamond by CVD used H_2/CH_4 as precursors, and polycrystalline diamond films were usually obtained. Some researchers have studied the effect of nitrogen addition in this system. It was found that a small amount of nitrogen could improve the diamond growth rate,[19] and promote the (100) preferred orientation,[20,21] while excessive nitrogen could distort the diamond structure and resulted in finer grains.[21,22] However, all the effects are still not fully explained. Our results reveal the behavior of this system from a different prospect, i.e., additional hydrogen into the N_2/CH_4 system. It is found that the pure N_2/CH_4 system yields nanocrystalline diamond films, and an additional small amount of hydrogen can increase the diamond grain size and lower the film growth rate. We have also noticed a promotion of diamond (111) orientation with increasing H_2 concentration from Fig. 6(b). These features of the $N_2/H_2/CH_4$ system are self supportive.

It is well known that CH_3 is the species responsible for the CVD diamond growth in the H_2/CH_4 system. The atomic H plays key roles in this process, such as etching off nondiamond phase, and stabilizing the growing surface by saturating the dangling carbon bonds, and the making it easy to grow large-size diamond crystallites.[17] In contrast, in the N_2/CH_4 environment, the concentration of atomic H is very low, and the diamond-growth species also varies from that for the H_2/CH_4 system. We have studied the chemical composition of our N_2/CH_4 plasma by optical emission spectroscopy. There are strong bands from species such as C_2, CN, and HCN, while the signals from atomic H are very weak. We believe that C_2 dimer, instead of CH_3, is the diamond-growth species in the N_2/CH_4 system. Unlike CH_3,C_2 dimer itself does not contain H atoms, so the C_2 growth surface is rich of vacancies and dangling carbon bonds. This gives an opportunity for the second and higher order nucleation, resulting in the formation of nanocrystalline diamond. It is known that atomic H plays a role in stabilizing the diamond surface. When a small amount of hydrogen gas is introduced, therefore, the diamond grain size will increase with increasing H_2 flow rate. This is consistent with our experimental results. Furthermore, when the H_2 concentration is comparable to that of N_2, the C_2 growth mechanism may compete with the CH_3 growth mechanism, resulting in no film growth. In order to fully explain the mechanisms in this process, more effort is needed to study the role played by CN and HCN in this process, and how the two growth mechanisms compete/interact with each other.

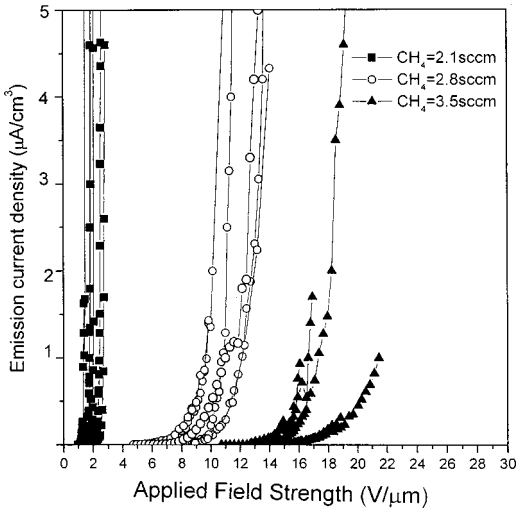

FIG. 11. FEE $I-V$ characteristic of nanocrystalline diamond films grown using CH_4/N_2 as precursors, with CH_4 flow rate ranging from 2.1 to 8.4 sccm.

E. Field emission properties and a transport-tunneling mechanism

Figure 11 shows the characteristic curve of the emission current versus the applied field for the films grown with only CH_4/N_2 as precursors. Different CH_4 flow rates of 2.1, 2.8, 3.5, 4.9, 6.3, and 8.4 sccm were used. It is found that with decreasing CH_4 concentration, the FEE properties of the films are significantly improved. When the CH_4 flow rate is decreased from 3.5 to 2.1 sccm, the emission threshold required to extract 1 nA emission current with the 1 mm^2 tip area drops from 15 to 1 V/μm. At the same time, the maximum emission current obtained in the films increases from 0.5 to 10 mA/cm^2. The results from the films grown with CH_4 flow rate higher than 4.9 sccm are not shown here, because there is no observable emission even when the applied field strength reaches 30 V/μm (the upper limit of our high voltage supply). It is noteworthy that the FEE result obtained in the film grown with 2.1 sccm CH_4 is among the best up to date[6,7,13,14] especially since our present results are measured on surfaces without any treatment. Figure 12 shows the corresponding Fowler–Nordheim (FN) plots, which can be well fitted by straight lines, indicating that the field emission property can be explained by a tunneling mechanism.

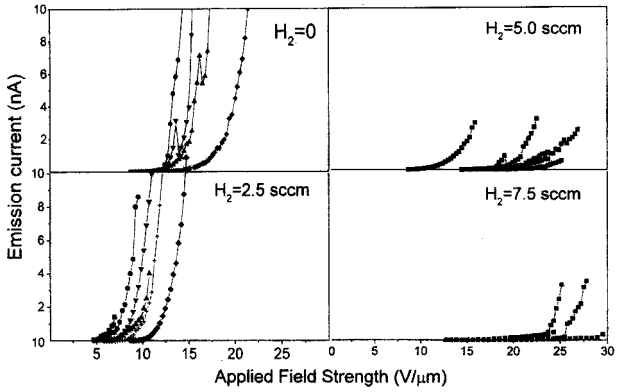

FIG. 13. FEE $I-V$ characteristic of nanocrystalline diamond films grown by adding (a) 0, (b) 2.5 sccm, (c) 5.0 sccm, and (d) 7.5 sccm H_2 to the N_2/CH_4 precursors.

Figure 13 shows the $I-E$ characteristics of the films grown with 0, 2.5, 5.0, 7.5, and 10 sccm H_2, in which the CH_4 was fixed at 3.5 sccm. The emission properties of these films show some improvement at the beginning when the H_2 flow rate increases from 0 to 2.5 sccm, but soon drops with further increase of H_2. In the film grown with 5.0 and 7.5 sccm H_2, the emission threshold becomes rather high, and the maximum emission current decreases significantly. Furthermore, in the film grown with 10 sccm H_2, there is no observable emission even when the applied field strength reaches 30 V/μm. Figure 14 shows the FN plot of the same films, where the same trend is displayed.

In order to explain the FEE mechanism of nanocrystalline diamond, a model based on the graphite/nanodiamond mix-phase structure is proposed. All the films used for FEE measurements in our experiment were grown on molybdenum substrates. In such a structure, graphite plays the role of

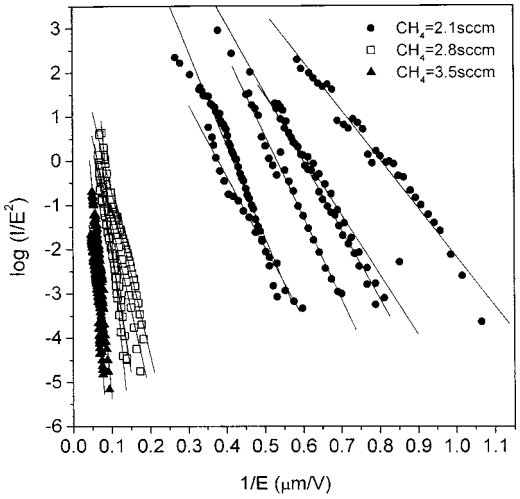

FIG. 12. FN plot of the field emission from the films grown with different CH_4 concentrations.

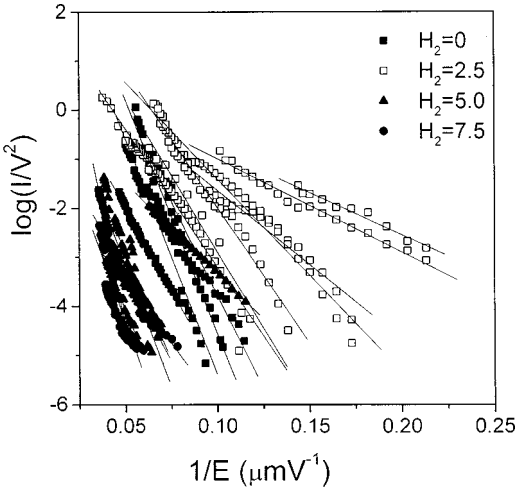

FIG. 14. FN plot of the field emission from the films grown with different H_2 flow rates.

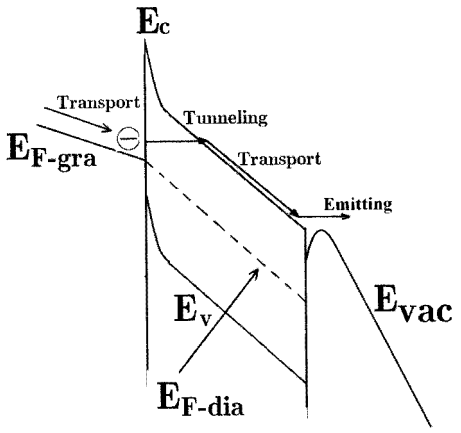

FIG. 15. Schematic diagram of field electron emission from a diamond/graphite mixed phase structure.

conducting channels from the Mo substrate to the film surface. While on the surface, we assume that the nanodiamond has a relatively low or even NEA as that of bulks. Thus electrons will first tunnel through the nearby diamond edges and then emit from the diamond surface, as suggested by Xu[2] and Geis.[23] Figure 15 shows a schematic diagram of this process. Here we assume that the electrons are only emitted from regions close to the particle edges, so further experimental evidence is still needed to demonstrate that the emission originates from the conduction band. In our model there are two main factors deciding the FEE property: (1) the diamond grain size, and (2) the graphite content in the film. As electrons from the diamond/graphite interface must tunnel through a barrier between them, the diamond grain size is a critical factor determining the tunneling probability. For large-size diamond grains, electrons can only be emitted from regions close to crystal edges, which are thin enough for electrons to tunnel through [Fig. 16(a)]. In contrast, for small-size diamond grains, electrons can be effectively emitted from a larger surface area, or even the whole diamond surface, thus greatly increasing the emission site density [Fig. 16(b)]. The graphite content is another critical factor because the emission starts from the diamond/graphite interface. There is an optimum graphite content for maximizing the graphite/diamond interface area on the film surface. The optimal value is when the graphite content is just enough to fill the gaps between the densely agglomerated diamond grains. Above this value, a decrease in graphite content will increase the diamond/graphite interface area, and thus enhance FEE. But when the graphite content is below this value, i.e., it is not enough to fill the gaps, a decrease in graphite content will decrease the interface area at the surface, and the field emission properties will drop. Moreover, further decrease of the graphite content will make it insufficient to form conducting channels, thus the emission properties will be rapidly degraded.

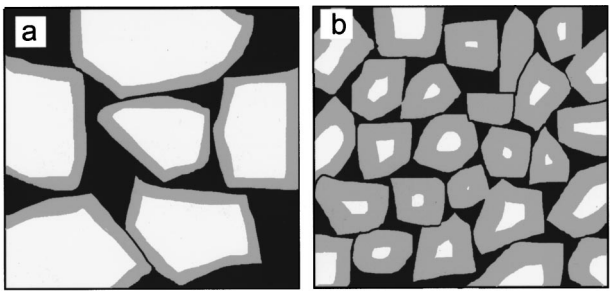

FIG. 16. View of the interface density of the diamond/graphite mixed phase structure. (a) shows a film with large diamond grain size, and (b) shows a film with small diamond size for comparison.

Based on the above model, our experimental results can be understood in the following way. As to the first series of the films grown without H_2, with the decrease of CH_4 concentration: (a) the diamond grain size becomes larger, from about 8 to 20–30 nm; and (b) the graphite content is reduced from about 40% to a lower value. The increase of diamond grain size has a negative effect on FEE. Since the change is not significant, this effect is relatively small. A decrease in the graphite content, on the other hand, has a positive effect on FEE. Combining these two effects, we believe that the positive effect of the decreasing graphite content cancels the negative effect introduced by increasing grain size, so the FEE property is improved.

As to the other series of films grown with H_2, with the increase of H_2 flow rate from 0 to 10 sccm, the diamond grain size increases from 8 to about 50 nm. The negative effect to FEE is similar to the previous case, but the larger grain size has a stronger effect. At the same time the graphite content decreases very much with increasing H_2. It has been revealed that the films grown with higher H_2 concentration have little graphitic phase by TEM and Raman. At the beginning, i.e., when the graphite content is still high, the decreasing graphite content has a positive effect on FEE, thus the FEE property of the films may be improved as a result of the combined effect of grain size and graphite content, which is seen in our experiment. But after this point, the graphite content drops below the optimum value, and thus a continuous decrease in the graphite content results in a strong negative effect, so the field emission properties of the films rapidly degrade as a consequence of the combined effect.

It should be noted that the FEE mechanism of nanocrystalline diamond film differs from that of polycrystalline films. As the diamond grain size is reduced to nanoscale, the conducting pathway formed by graphite in the crystal boundaries is enhanced by hundreds of times, which greatly increases the film conductivity. Furthermore, nanocrystalline diamond films have nanoscale smooth surfaces, implying a much lower field enhancement factor than that of rough polycrystalline diamond surfaces. As Bandis *et al.* have pointed out because polycrystalline diamond films can have field enhancement factors on the order of 10^2, the high electric field can even cause electrons to emit from the valance band of diamond.[24,25]

IV. CONCLUSION

In conclusion, nanocrystalline diamond films were obtained by a MPCVD using a new combination of $N_2/CH_4/H_2$ precursors. The microstructure of the films was controlled by the CH_4 concentration and/or additional of H_2 into the precursors. The growth mechanism of nanocrystalline diamond

films grown by such a system can be understood in terms of the surface stabilizing model. The films grown with optimized parameters present novel field emission properties, such as 1 V/μm emission threshold and 10 mA/cm^2 emission current. The field emission properties of our nanocrystalline diamond films can be explained by a conducting–tunneling mechanism, in which graphite plays an important role in the electron emitting process. These results show that CVD deposited nanocrystalline diamond films can be a more promising cold cathode material for future FEE applications.

ACKNOWLEDGMENTS

This work was supported by the Chinese Academy of Sciences, the State Key Project of Fundamental Research, and the NSF of China.

[1] F. J. Himpsel, J. A. Knapp, J. A. VanVechten, and D. E. Eastman, Phys. Rev. B **20**, 624 (1979).
[2] N. S. Xu, Y. Tzeng, and R. V. Latham, J. Phys. D **26**, 1776 (1993).
[3] Y.-H. Chen, C.-T. Hu, and I.-N. Lin, J. Appl. Phys. **84**, 3890 (1998).
[4] M. W. Geis, J. C. Twichell, N. N. Efremow, K. Krohn, and T. M. Lyszczarz, Appl. Phys. Lett. **68**, 2294 (1996).
[5] T. Yamada, H. Ishihara, K. Okano, S. Koizumi, and J. Itoh, J. Vac. Sci. Technol. B **15**, 1678 (1997).
[6] K. Okano, S. Koizumi, S. Ravi, P. Silva, and G. A. J. Amaratunga, Nature (London) **381**, 140 (1996).
[7] W. Zhu, G. P. Kochanski, and S. Jin, Science **282**, 1471 (1998).
[8] N. Kumar and H. Schmidt, Semicond. Sci. Technol. **71**, 73 (1995).
[9] A. Wisitsora-at, W. P. Kang, J. L. Davidson, and D. V. Kerns, Appl. Phys. Lett. **71**, 3394 (1997).
[10] P. W. May, S. Hohn, M. N. R. Ashfold, W. N. Wang, N. A. Fox, T. J. Davis, and J. W. Steeds, J. Appl. Phys. **84**, 1618 (1998).
[11] V. F. Dorfman, Thin Solid Films **212**, 267 (1992).
[12] D. M. Bhusari, J. R. Yang, T. Y. Yang, S. T. Lin, K. H. Chen, and L. C. Chen, Solid State Commun. **107**, 301 (1998).
[13] D. Zhou, A. R. Krauss, L. C. Qin, T. G. McCauley, D. M. Gruen, T. D. Corrigan, R. P. H. Chang, and H. Gnaser, J. Appl. Phys. **82**, 4546 (1997).
[14] D. Zhou, A. R. Krauss, T. D. Corrigan, T. G. McCauley, R. P. H. Chang, and D. M. Gruen, J. Electrochem. Soc. **144**, L224 (1997).
[15] Kehui Wu, E. G. Wang, J. Chen, and N. S. Xu, J. Vac. Sci. Technol. B **17**, 1059 (1999).
[16] A. Guinier, *X-Ray Diffraction* (W. H. Freeman, San Francisco, 1963), p. 121.
[17] W. A. Yarbrough and R. Messier, Science **247**, 3842 (1990).
[18] A. A. Talin, L. S. Pan, K. F. McCarty, and T. E. Felter, Appl. Phys. Lett. **69**, 3842 (1996).
[19] W. M. Sebert, E. Worner, F. Fuchs, C. Wild, and P. Koidl, Appl. Phys. Lett. **68**, 759 (1996).
[20] R. Locher, C. Wild, N. Herres, D. Behr, and P. Koidl, Appl. Phys. Lett. **65**, 34 (1994).
[21] S. Jin and T. D. Mowtakas, Appl. Phys. Lett. **65**, 403 (1996).
[22] S. Bohr, R. Hanbner, and B. Lov, Appl. Phys. Lett. **68**, 1075 (1996).
[23] M. W. Geis, J. C. Twichell, and T. M. Lyszczarz, J. Vac. Sci. Technol. B **14**, 2060 (1996).
[24] C. Bandis and B. B. Pate, Appl. Phys. Lett. **69**, 366 (1996).
[25] K. Okano, T. Yamada, A. Sawabe, S. Koizumi, R. Matsuda, C. Bandis, W. Chang, and B. B. Pate, Appl. Surf. Sci. **146**, 274 (1999).